The sound of geological targets on Mars from the absolute intensity of laser-induced sparks shock waves

C. Alvarez-Llamas, J. Laserna, J. Moros, P. Purohit, L. García-Gómez, S.M. Angel, P. Bernardi, B. Bousquet, A. Cadu, E. Dauson, et al.

Spectrochimica Acta Part B: Atomic Spectroscopy 205 (2023) 106687

Contents lists available at ScienceDirect

Spectrochimica Acta Part B: Atomic Spectroscopy

journal homepage: www.elsevier.com/locate/sab

The sound of geological targets on Mars from the absolute intensity of laser-induced sparks shock waves

C. Alvarez-Llamas [a], J. Laserna [a,*], J. Moros [a], P. Purohit [a], L. García-Gómez [a], S.M. Angel [b], P. Bernardi [c], B. Bousquet [d], A. Cadu [e], E. Dauson [f], O. Forni [g], T. Fouchet [c], O. Gasnault [g], X. Jacob [h], G. Lacombe [g], N.L. Lanza [f], C. Larmat [f], J. Lasue [g], R.D. Lorenz [i], P.-Y. Meslin [g], D. Mimoun [e], F. Montmessin [j], N. Murdoch [e], A.M. Ollila [f], P. Pilleri [g], N. Randazzo [k], A.L. Reyes-Newell [f], S. Schröder [l], A. Stott [e], J. Ten Cate [f], A. Udry [m], D. Vogt [l], S. Clegg [f], A. Cousin [g], S. Maurice [g], R.C. Wiens [n], the SuperCam Acoustics and LIBS Working Groups

[a] *Departamento de Química Analítica, Universidad de Málaga, Málaga, Spain*
[b] *Department of Chemistry and Biochemistry, University of South Carolina, Columbia, SC, USA*
[c] *Laboratoire d'Etudes Spatiales et d'Instrumentation en Astrophysique, Observatoire de Paris-PSL, CNRS, Sorbonne Université, Université de Paris Cité, Meudon, France*
[d] *Centre Lasers Intenses et Applications, CNRS, CEA, Université de Bordeaux, Bordeaux, France*
[e] *Institut Supérieur de l'Aéronautique et de l'Espace (ISAE-SUPAERO), Université de Toulouse, SAE-SUPAERO, Toulouse, France*
[f] *Los Alamos National Laboratory, Los Alamos, NM, USA*
[g] *Institut de Recherche en Astrophysique et Planetologie (IRAP), Université de Toulouse 3 Paul Sabatier, UPS, CNRS, CNES, Toulouse, France*
[h] *Institut de Mécanique des Fluides, Université de Toulouse 3 Paul Sabatier, Institut National Polytechnique de Toulouse, Toulouse, France*
[i] *Johns Hopkins University Applied Physics Laboratory, Laurel, MD, USA*
[j] *Laboratoire Atmosphères, Milieux, Observations Spatiales, CNRS, Université Saint-Quentin-en-Yvelines, Université Paris Saclay, Sorbonne Université, Guyancourt, France*
[k] *University of Alberta, Edmonton, Canada*
[l] *Deutsches Zentrum für Luft- und Raumfahrt (DLR), Institute of Optical Sensor Systems, Berlin, Germany*
[m] *University of Nevada, Las Vegas, NV, USA*
[n] *Earth, Atmospheric, and Planetary Sciences, Purdue University, West Lafayette, IN, USA*

ARTICLE INFO

Keywords:
Acoustics
Mars
Perseverance
Jezero
LIBS
Geological material

ABSTRACT

Inspection of geological material is one of the main goals of the Perseverance rover during its journey across the landscape of the Jezero crater in Mars. NASA's rover integrates SuperCam, an instrument capable of performing standoff characterization of samples using a variety of techniques. Among those tools, SuperCam can perform laser-induced breakdown spectroscopy (LIBS) studies to elucidate the chemical composition of the targets of interest. Data from optical spectroscopy can be supplemented by simultaneously-produced laser-produced plasma acoustics in order to expand the information acquired from the probed rocks thanks to the SuperCam's microphone (MIC) as it can be synchronized with the LIBS laser. Herein, we report cover results from LIBS and MIC during Perseverance's first 380 sols on the Martian surface. We study the correlation between both recorded signals, considering the main intrasample and environmental sources of variation for each technique, to understand their behavior and how they can be interpreted together towards complimenting LIBS with acoustics. We find that louder and more stable acoustic signals are recorded from rock with compact surfaces, i.e., low presence loose particulate material, and harder mineral phases in their composition. Reported results constitute the first description of the evolution of the intensity in the time domain of shockwaves from laser-produced plasmas on geological targets recorded in Mars. These signals are expected contain physicochemical signatures pertaining to the inspected sampling positions. As the dependence of the acoustic signal recorded on the sample composition, provided by LIBS, is unveiled, the sound from sparks become a powerful tool for the identification of mineral phases with similar optical emission spectra.

* Corresponding author.
E-mail address: laserna@uma.es (J. Laserna).

https://doi.org/10.1016/j.sab.2023.106687
Received 14 March 2023; Received in revised form 18 April 2023; Accepted 18 April 2023
Available online 20 April 2023

1. Introduction

In February 2021, in the context of the Mars2020 mission, the Perseverance rover (Fig. 1A) landed in Jezero crater, Mars, precisely at the landing site named Octavia E. Butler (OEB). The crater is located near the western edge of *Isidis Planitia* and east of *Nili Fossae* in Noachian terrain (18.4°N 77.5°E). OEB is located ~2.2 km SE of a sedimentary fan Fig. 1B (inset), recently confirmed as a delta deposited within a lake with fluctuating water levels [1]. The Mars 2020 mission has four specific objectives: 1) to develop a scientific understanding of the geology of Jezero crater, 2) to seek biosignatures that could help in the identification of ancient habitable environments, 3) to collect and document a suite of samples to be returned to Earth by a future mission and 4) to demonstrate pioneering technologies to enable future Mars exploration. Perseverance's scientific equipment consists of seven proximity and remote science instruments to accomplish these objectives. More information on the mission and the different instruments can be found in Farley et al. [4].

Among the instrument payload on Perseverance, SuperCam was developed to perform remote science observations to contribute to all four primary mission goals. It provides key information via a combination of several techniques, including Laser-Induced Breakdown Spectroscopy (LIBS), Time-Resolved Raman and Luminescence (TRR and TRL), Visible and near-Infrared spectroscopy (VISIR), high-resolution colour imaging (RMI), and sound recording using a microphone (MIC) [5,6]. The measurements provided by the SuperCam techniques, either individually or by merging two or more sources, allow to obtain geological and atmospheric information about the Martian surface. LIBS has been used to acquire compositional information concerning the Martian surface since 2012 as part of the ChemCam instrument for NASA's Mars Science Laboratory mission [7,8], the SuperCam instrument in NASA Perseverance rover since Feb 18, 2021 [5,6], and MarSCoDe as part of China's Tianwen-1 mission, which landed in May 2021 [9].

Furthermore, Perseverance has brought about the possibility of studying acoustics on Mars for the first time in human history. The microphone provided by SuperCam has been used to measure pressure fluctuations in the range from 20 Hz to 50 kHz. The results reported by Maurice et al. [10], were supported by recordings from both natural sources (i.e. atmosphere or dust devils [11,12]) and artificial sources. i.e., rover actuators and pumps, the oxygen-fabric compressor, the camera focus mechanisms, and the Ingenuity helicopter. It was specifically designed to record the shockwave generated by the plasma expansion during LIBS data acquisitions. More detailed information about the SuperCam instrument, including MIC and LIBS, can be found in [5,6].

The possibility of simultaneously acquiring spectroscopic data from LIBS and acoustic recordings from MIC using SuperCam on geological targets was demonstrated in a series of benchmark tests prior to the deployment of Perseverance on Mars [13,14]. The results reported a correlation between the relative acoustic energy and the ablated mass, as well as a relationship between the decay rate of the acoustic energy and the target hardness and density [14]. Moreover, studies about the possibility of discriminating mineral phases based on the acoustic plasma signal were proved in previous works [15,16].

In the present work, we present simultaneous LIBS and MIC results obtained by SuperCam during the first 380 Sols since its deployment. During this time, the rover has driven along Jezero crater's floor acquiring data over basaltic rocks of various compositions. A descriptive study is carried out, focusing on the possible sources of signal variations due to the environmental and physico-chemical characteristics of the inspected targets. The responses from both techniques are studied in order to correlate them to the traits of the inspected targets and to highlight trends according to the studied traits. We aim to associate the acoustic response to the sample's chemical composition extracted from LIBS. In doing so, acoustics may become a useful asset for complementing LIBS analysis of rocks, mainly in those cases for which targets with different origins or nature yield similar optical spectra.

2. Datasets

This study focuses on the initial part of the mission, the first 380 sols on Mars (a "Sol" is a solar day on Mars (88,775 s), and Perseverance landed on Sol 0).

Geological context From Sol 0 to Sol 380, Perseverance mainly traversed the intersection between two Crater-Fill Units labelled Crater floor fractured rough (Cf-fr, named Máaz), and Crater floor fractured 1 (Cf-f-1, named Séítah) [17]. Máaz is a crater-retaining unit which covers much of the Jezero crater floor. It has been described as a 'dark-toned soil' and mafic unit composed of erosion-resistant bedrock [17,18]. On the other hand, Séítah consists of massive light-toned units, classified as either part of the regionally extensive carbonate-bearing or the olivine-bearing units. Based on SuperCam measurements, several chemical differences were found between the units [19]. Máaz is characterized by a broad basaltic composition (a mixture of plagioclase and pyroxene, feldspar and Fe minor-oxides and apatite), while Séítah is dominated by olivine, with the overall composition exhibiting trends between pyroxene and olivine [19,20]. An exception to this general Séítah composition is the group of pitted, less crystalline rocks called "Content mb" (Fig. 1B), which present a lack of olivine and was compositionally similar to Máaz. Lastly, starting from Sol 177, SuperCam observed

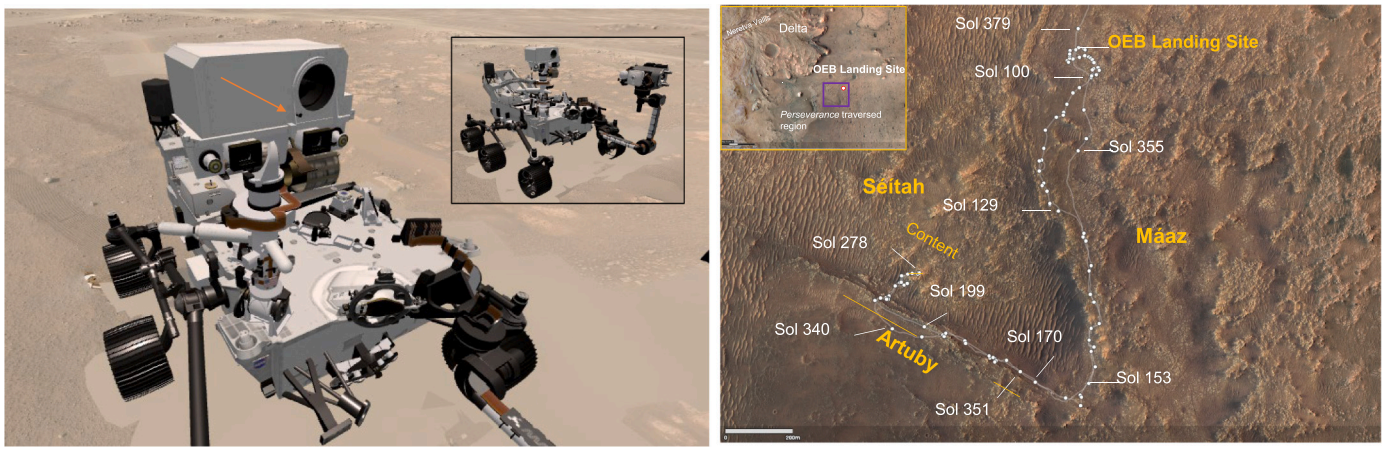

Fig. 1. A) Perseverance rover model [2]. Orange arrow points to SuperCam's Microphone. B) Rover transverse during the first 380 sols, with the rover position in white dots, and the geological features in yellow. The inset shows the position of this area with respect to the Jezero delta [3]. (For interpretation of the references to colour in this figure legend, the reader is referred to the web version of this article.)

variable recessive layered outcrops below the ridge nicknamed "Artuby" and massive outcrops at its top. A compositional trend from Máaz to Artuby to Séítah could be observed based on the % of oxides measured in each area. SiO_2, Al_2O_3, Na_2O, and K_2O were found to decrease significantly, with notably lower alkali and higher MgO in Séítah. This revealed an increasing progression of mafic materials and, subsequently, density [19]. Further information can be found in the works by Stack et al. [17], S. Holm-Alwmark et al. [18] and Wiens et al. [19].

Rock and soil compositions. The LIBS laser is a compact active Nd: YAG Q-switched source delivering ~15 mJ pulse energy (at $\lambda = 1064$ nm) over a spot of 250–400 μm (Irradiance >10 MW mm^{-2} up to 7 m) at the target surface. The spectral range of the spectrometers is 243–853 nm, featuring two wavelength gaps between 340 and 382 and 467–535 nm. The detection is based on two f/4 Crossed Czerny-Turner coupled to CCDs for the ultraviolet to blue-violet ranges and a transmission spectrometer coupled to an ICCD for the 535–853 nm range. More detailed technical information about the LIBS instrument can be found in Wiens et al. and Maurice et al. [5,6]. Elemental compositions of the interrogated targets are obtained from LIBS as oxides (SiO_2, TiO_2, Al_2O_3, FeO_T, MgO, CaO, Na_2O, K_2O) by implementing different chemometric analytical tools on the acquired emission spectra [19]. This involves a library of >320 standards. The quantitative elemental values used in the present work have been calculated by the SuperCam Science Team using the above-mentioned methodology. The accuracy/precision for the prediction model on the major oxides are (in weight percent): 6.1/1.6, 0.3/0.02, 1.8/0.7, 3.1/1.3, 1.1/0.5, 1.3/0.5, 0.5/0.3, 0.6/0.3% for SiO_2, TiO_2, Al_2O_3, FeO_T, MgO, CaO, Na_2O, K_2O, respectively [19].

Acoustic data. SuperCam's microphone records pressure fluctuations from 20 Hz to 50 kHz, at a sampling rate of 100 kHz, with a sensitivity of 29.6 mV Pa^{-1} at 1 kHz without amplification. The microphone is synchronized to the laser pulses, recording a time of 60 ms around the laser shot (the laser repetition rate itself is at 3 Hz, so there is a data gap between two consecutive recordings). Initially planned to record laser-induced shockwave up to 4 m, successful recordings were obtained up to 9.2 m [5,6].

Observations along the rover traverse. The nearly 380 sols considered in the present work comprise >62 k different LIBS spectra and > 60 k acoustic recordings from 1907 sampling positions. Hence, 234 different targets have been sampled, each observed between 5 and 10 times along what is called a raster. 30 Laser shots are used at each position, and occasionally 150 shots. Each laser shot is recorded by both techniques, except for the last shot on acoustics for technical reasons (that explains the difference between the number of laser shots and MIC recordings). There are 6 types of targets:

- *Bulk* (*67%* of the acoustic analyzed targets). Rocks are at least centimeter-size, that is significantly larger than the laser-matter interaction area.
- *Abraded patch (10%)*. Rock surfaces that have been abraded by the rover during the studies related to collecting samples to be returned back to Earth and are considered separately.
- R*egolith (10%)*, sand and soil, in general, with characteristic granules whose sub-millimeter size is close to the diameter of the laser spot (300–600 μm), were considered as a group.
- *Drill tailings (2%)* are generated during the drilling process. This "*tailings*" group represent an extreme example of pulverized targets due to their minimal compaction.
- A Ti plate (*6%*). Standard material integrated as a part of the SuperCam calibration target (SCCT) and used for wavelength calibration. These observations were not used in this study due to the large differences in nature (metal plate vs rock) and placement (located on the rover itself).
- *Drill Hole (5%)*. Measurements within the drill hole after sample collection. The targets were not used because of the expected acoustic changes induced by the hole.

Fig. 3 a-e presents some examples of the different targets using the classification mentioned above (Annex 1 in the Supplementary data provides the links to the image sources). These panels illustrate the types of targets detailed in Fig. 2. Given the outlined particularities of the acoustic acquisition environment for the Ti plate and the Sample Collection Hole data, they cannot be compared to the rest of the observations and, therefore, will not be considered in this study. Targeting Position (red crosses in Fig. 3) refers to the number of positions analyzed considering all the targets, whereas sequence refers to a set of analyses performed at one or several positions in one target (each image in Fig. 3 corresponds to a sequence).

3. Data processing

Acoustic data in digital number (DN) are first converted to pressure units (Pa), then, the signals, 60 ms per laser shot, are filtered with a bandpass filter between 2 and 15 kHz, as earlier studies [13] have shown that this region contains >95% of the acoustic energy from the laser-induced shock wave. The peak-to-peak amplitude of the first compression-rarefaction in the acoustic wave is extracted as an analytical signal. Such a signal, hereinafter called "acoustic signal", corresponds to the amplitude of the acoustic wave between the first maximum and the first minimum (represented in the inset of Fig. 4b). From Pa, signal values were converted in dB according to the expression:

$$dB = 20log_{10}P/_{P'}$$

Where P' is the reference pressure value for Earth, i.e., $P' = 20$ μPa.

An immediate question arising from the analyses herein reported is the possibility of supplementing the results and conclusions drawn from inspecting the sound pressure with their corresponding data in the frequency domain. Frequencies are expected to expand the sample description owing to their connection with the chemistry of the different mineral phases constituting the rock under study [21]. Yet, tests performed under tightly controlled in-lab scenarios have shown that the complete sound wave is largely impacted by the surroundings of the sample [21,22]. As physical obstacles (orography, close pebbles, …) and atmospheric conditions may vary largely between the inspection events under evaluation, the associated echoes and interferences seeding variability to the complete time acoustic wave translate into artifacts to the frequency domain. Unfortunately, since the peak-to-peak amplitude of the first compression-rarefaction used herein (less vulnerable to echoes and interferences due to their later arrival times) is built from a small number of data points, it does not provide sufficient resolution to the acoustic response when transformed to the frequency domain.

Variation of the acoustic properties of the atmosphere. During the first 380 sols (1 Martian year ~668.6 sols), the meteorology on Mars changed significantly. The solar longitude (L_s) at this period goes from 5°-191°. The L_s measures the Mars position in its orbit about the sun. The 0°, 90° and 180° correspond to the northern spring equinox, summer solstice and autumnal equinox, respectively. The temperature and pressure changes induced subsequent modifications in the propagation of the acoustic wave through the atmosphere due to an alteration in the instantaneous acoustic impedance [23]. The impedance conditions of the medium strongly influence the variation of the acoustic signal over time. Fig. 4a represents data with and without the impedance correction, showing that a large number of raw data are underestimated without this correction due to the impedance evolution during this period. In order to correct the influence of this variation on the acquired signals, the acoustic signal is corrected by the variation of the impedance value with respect to the first acoustic measurement (Sol 37).

Distance correction for acoustic data. As mentioned above, targets analyzed by SuperCam were located at distances ranging from 2 m to 9 m from the instrument, resulting in various atmospheric column densities along the acoustic path. In order to readily compare the different acoustic signals, a distance correction factor was applied. The

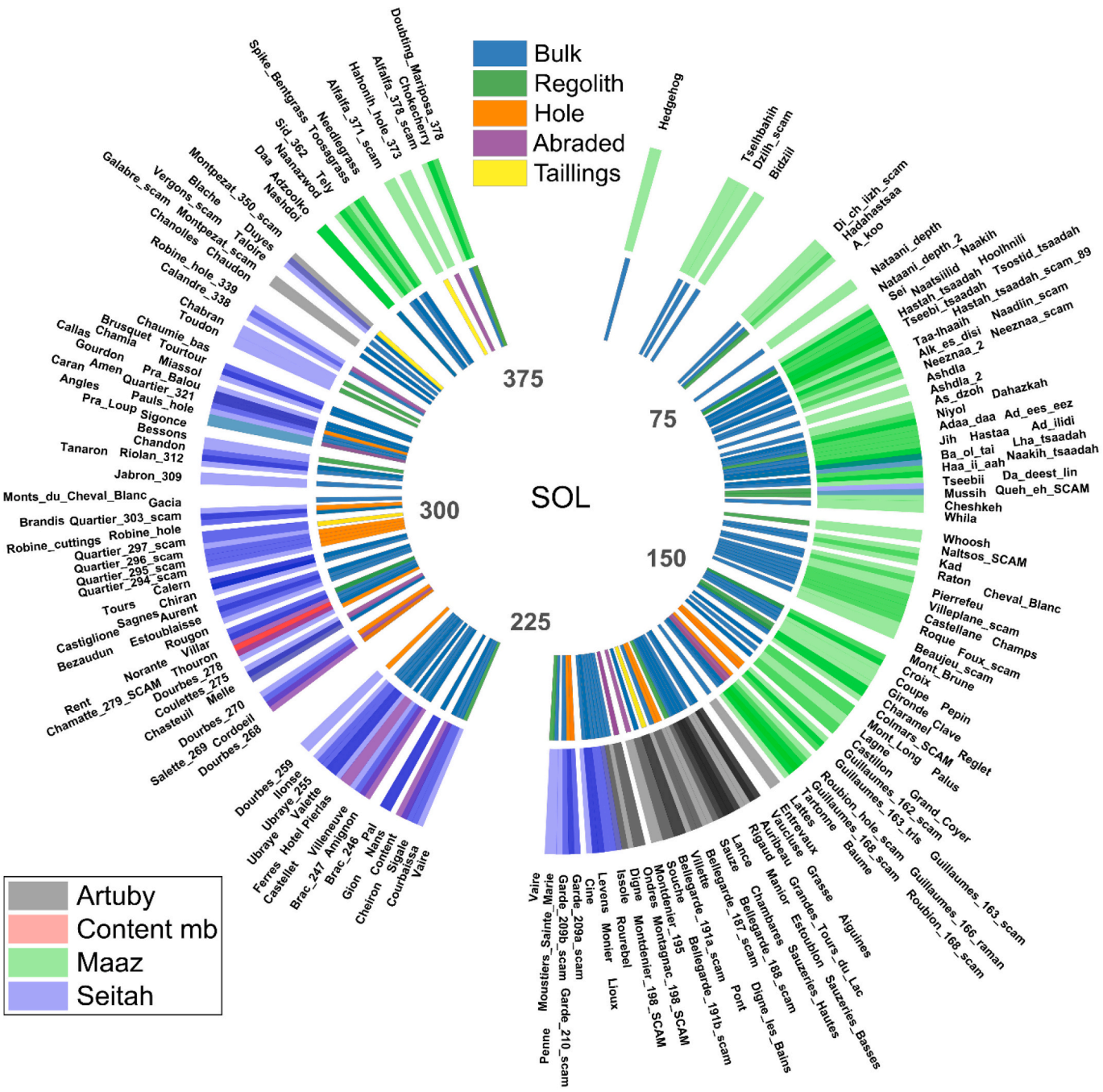

Fig. 2. Schematic representation of the targets analyzed using simultaneous LIBS + MIC measurements by SuperCam. The angular position represents the execution sol. The internal colored circle (top legend) identifies the type of target, and the external-colored circle (bottom-left legend) associates the target to its corresponding geological unit.

atmospheric attenuation can be modelled using the expression $f(r) = k.\ r^{-1}r^{-0.698}e^{-\alpha r}$, where r^{-1} represents the spherical wave propagation, $r^{-0.698}$ the decrease of the laser irradiance with distance [6], and $e^{-\alpha r}$ the acoustic wave's excess attenuation due to atmospheric absorption [10]. Fig. 4b shows the decay curve with the distance, as well as the smoothed signal obtained (15 points average smooth). These values were fitted to $f(r)$ to obtain $\alpha = 0.289\ m^{-1}$ ($CI_{95\%}$ (0.284, 0.294)) for the excess attenuation coefficient and $k = 4.61$($CI_{95\%}$ (4.55, 4.67)) for the constant. The attenuation coefficient is frequency-dependent.Considering the half-period between the maximum and minimum peaks of the acoustic wave, we can estimate the acoustic frequency to 8.5 ± 1.7 kHz. The attenuation calculated between 1 m and 2 m is −10 dB. This value is in concordance with that found in the literature, −9 dB at 8 kHz [10].

Variability of acoustic data. Strong temperature gradients along the acoustic path directly affect the propagation time and the shot-to-shot variability of the recorded signal and the MIC precision. This was addressed in detail by Chide et al. [11]. Fig. 4c.1 represents the relative standard deviation (RSD) of the acoustic signal at different local mean solar times (LMST) for targets located at distances from 2 m to 7 m. The largest RSD was found in the range from 11:00 to14:00, when thermal fluctuations due to atmospheric turbulence are maximum [11]. Unfortunately, most of the SuperCam recordings were carried out at this time (Fig. 4c.2).

Furthermore, the acoustic signal RSD (Fig. 4d) is almost three-fold

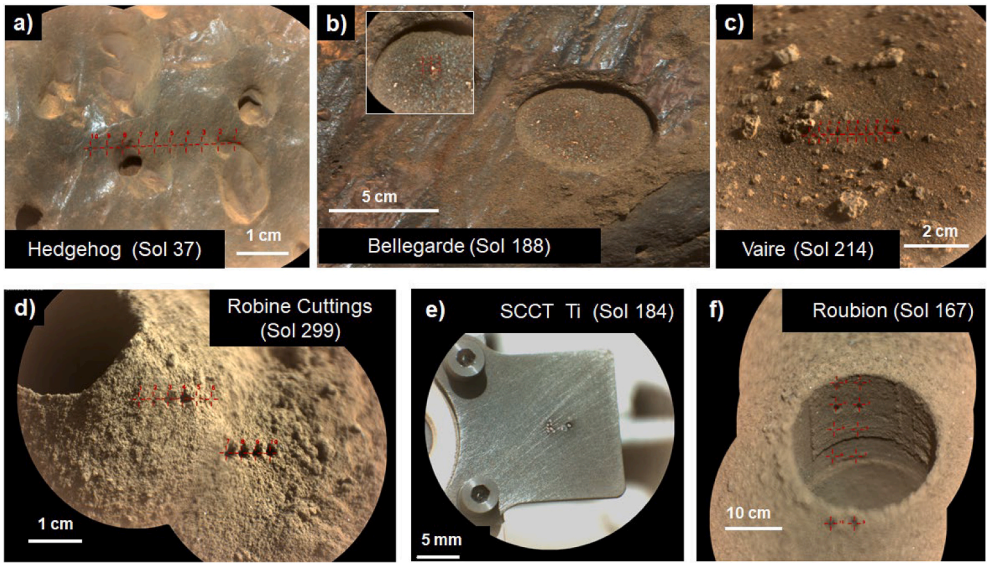

Fig. 3. Image of several examples for a) Bulk targets; b) Abraded patch; c) Regolith; d) Drill Tailings; e) Titanium SCCT, and f) Sample Collection Hole. The black labels represent the target name, and the red crossed the LIBS sampling position. Links to the images: Annex I on the Supplementary material document. (For interpretation of the references to colour in this figure legend, the reader is referred to the web version of this article.)

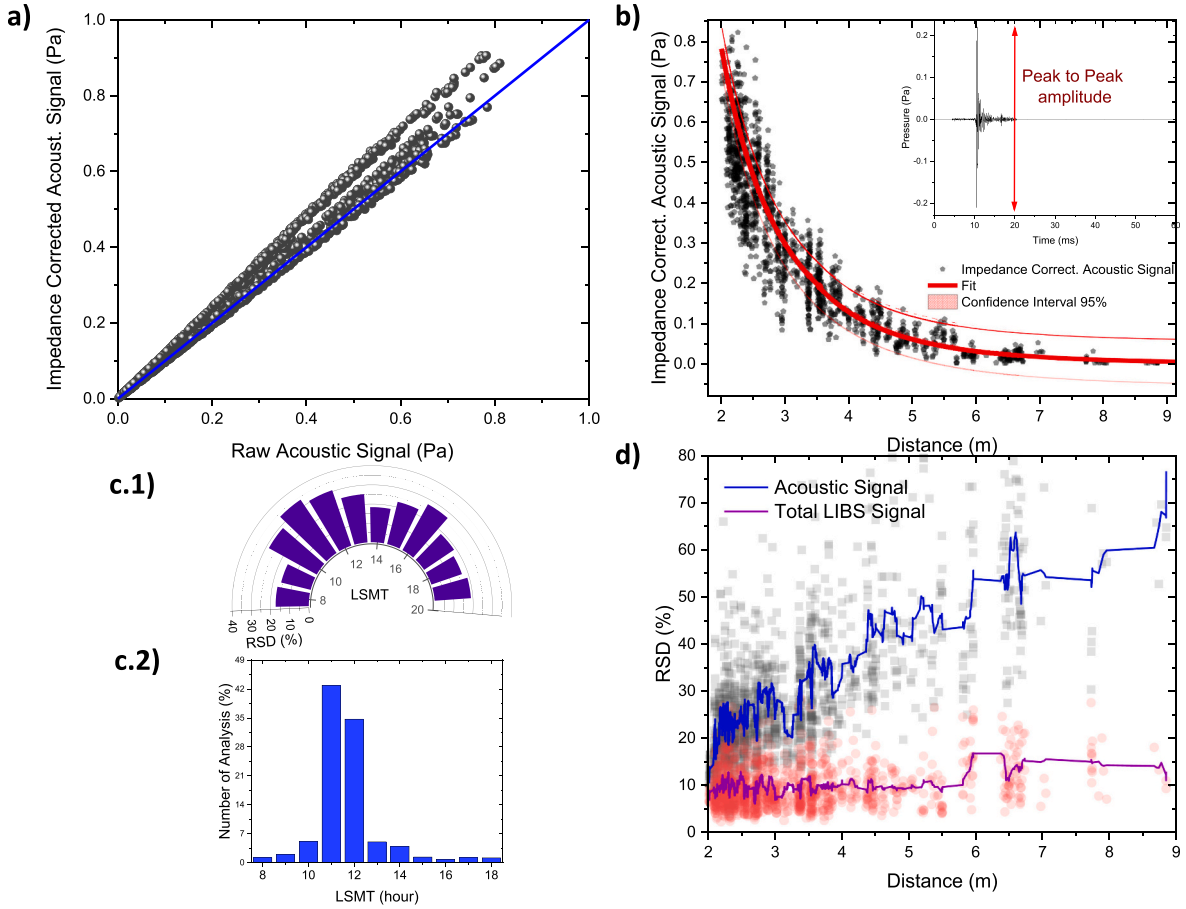

Fig. 4. Sources of LIBS and MIC signal variations. a) Raw vs Impedance-corrected acoustic signals (blue line corresponds to x = y). b) Decrease of the acoustic signal with respect the sample distance, with the fitting curve in red. c) Influence of the daily time on the acoustic signal RSD (intra-position), as well as the number of analysis for each temporal slot. d) Influence of the distance on the intra-position %RSD for the acoustic and LIBS signals. The solid line guides the trend identified for the RSD of both gathered acoustic and optical responses from the targets' inspection with the increase of the distance at which they are located. (For interpretation of the references to colour in this figure legend, the reader is referred to the web version of this article.)

larger at the distant targets than at the closest ones. This can be attributed to the effect of the short-term variation during the sound propagation through the Martian atmosphere. Overall, we find RSD values ranging from 20% to 70%.

Variability of LIBS data. The total emission of the LIBS spectra is used to track the variability of LIBS data and its evolution with target distance. Fig. 4d shows that shot-to-shot variability has an RSD of around 10%. Despite the decreases in the laser irradiance and the efficiency of the collection as a function of distance [6], we find no significant bias with distance. Note that shot-to-shot analysis (at the same position) as well as point-to-point analysis within the same target surface may induce signal intensity variations because of the target compositions.

4. Results and discussion

From the considered dataset, we investigated to what extent the absolute intensity of the sound may be modulated by factors including 1/ the quality of the focus, 2/ the rock hardness, 3/ the size of grains in soils, 4/ variations between geologic units and their chemistry.

Focal Influence. The laser-to-target distance may change significantly during the raster analysis, in most cases due to changes in target geometry. Usually, SuperCam adjusts the focus at the raster's center and at the extreme positions, so several points inherit the focusing of another position and, therefore, might fall out of focus. Fig. 5 presents a violin plot showing the relationship of acoustic variation to focal position.

The acoustic variation (AV) refers to any variation between the acoustic signal from non-focused points (AcS) and the previous focal one (AcS_f) computed as $AV = (AcS - AcS_f)\,AcS_f^{-1}$. The x-axis presents the variation of the focal distance in %. The selected values correspond to the percentiles 20, 40, 50, 60, 100. The mean signal (magenta line) shows the mean value for each plot; however, the points have a greater dispersion with respect to the null value. Since wider regions of the density plot indicate those values that occur more frequently, and mainly in all cases these regions lie close to zero, it is possible to conclude that the focal change does not appear to have a substantial influence on the variation of the acoustic signal. It should be noted that the fact that a point is categorized as "non-focal" is not synonymous with it being "out of focus"; it simply means that the focus was not checked at that particular point. So, in light of the information, it is expected that, under regular operation, any slight variation in focus does not severely disturb the acoustic signal.

Hard and soft surfaces. As expected, the recorded signals depend on

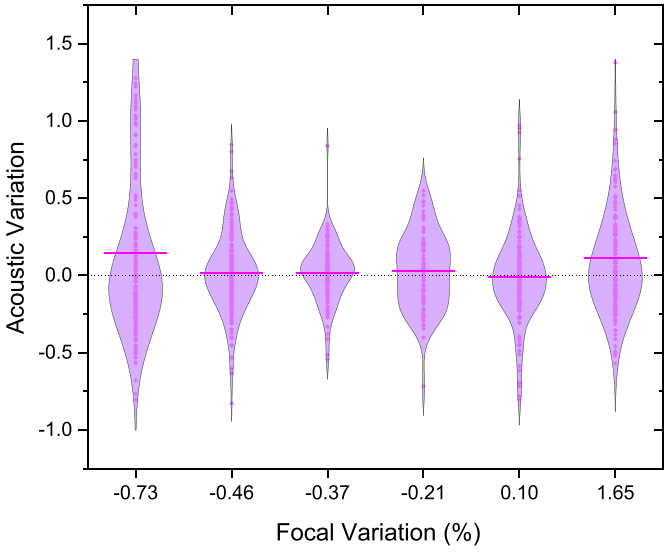

Fig. 5. Violin plot representing the acoustic variation as a function of the change in the focal position.

the structural and compositional characteristics of the analyzed rocks. Although SuperCam LIBS+MIC targets were categorized into 6 groups, only "bulk rock", "abraded patch", "regolith" and "drilling tailings" were considered for the presented studies. Fig. 6 uses different quantities to compare these four populations. Fig. 6a displays violin plots showing the relationship of the corrected acoustic signal to the type of target. Data reveals that consolidated surfaces, such as "bulk rocks" and "abraded patches" result in slightly stronger signals than loose ("regolith") materials and much louder signals than powdered ("tailings") targets. The acoustic signals of "tailings" present the lowest amplitude, with a decrease of 24 dB when comparing with the rock median acoustic signal. Indeed, the results from the "tailings" group and other previous within the associated literature correlate lower material compaction to lower acoustic signals [13]. The acoustic behavior, evaluated in terms of acoustic pressure (signal intensity) and acoustic slope (the variation of the signal intensity for a series of laser pulses performed at the same analysis position) for targets from "bulk" and "abraded" populations were not significantly different (at a 0.95 level). Proof of that is the computed mean RSD with values of 28% for "bulk" and 22% for "abraded" targets. The minimal differences observed could be attributable to the surface leveling caused during the abrasion process may be responsible, as "abraded" targets do not present the different surface orientations, pits or cracks identified in the "bulk" targets. In addition, for those "unconsolidated" targets, "regolith" targets provide more variable acoustic signals, whereas "tailings" exhibit a much smaller data dispersion. The variability of acoustic data identified for each type of target is reported in Fig. 6b, where the histograms show how frequently the intra-position relative standard deviation of the acoustic signals falls into a particular bin. Thus, the broad range of acoustic signals observed in the "regolith" can be argued by the variable size distribution of regolith grains and the presence of bigger pebbles acting similarly to consolidated surfaces during the laser interaction. In this line, Fig. S1 (provided as supplementary material) compares the variation of the averaged acoustic and LIBS slope per target population as well as the distribution of the acoustic-LIBS correlation values for the targets conforming to each population.

"Tailing" and "Regolith" targets. As discussed in the previous section, laser-driven acoustics for targets with a granular or less cohesive structure ("tailings" and "regolith") significantly differs from that of rock targets, either in intensity (a lower amplitude in the case of "tailings") or in stability (a broad range of amplitudes in the case of "regolith"). As this may indicate that further information could be extracted from these targets, observations related to those populations were further evaluated. Data in Fig. 7 shows the acoustic intensity for observations from both populations as well as the variation of the acoustic signal during the 29 first shots within each sampling position, computed from the slope of the acoustic signal versus the number of shots. Thus, a negative slope refers to acoustic signals featuring an intensity decrease trend as the laser shots drill the target. Furthermore, owing to the variability within "regolith" population, "fine" and "coarse" subclasses were differentiated based on a qualitative analysis of the high-resolution images acquired by SuperCam for each target. In addition, typical acoustic values for "bulk rocks" are shown for reference.

Comparing Geological Units Thus, the possible influence on the acoustic signal of the microparticulate material from a dust layer deposited over the target's surface prior to the laser scanning analysis was considered and evaluated. In this line, Fig. S2 (provided as supplementary material), shows high-resolution pictures provided by SuperCam's RMI of the precise locations over six targets presenting clear signs of dust removal, prior (left) and after (right) the laser shootings. In addition, a boxplot comparing the ratios between the mean value of the acoustic signals from the 3 first shots and the mean value of the acoustic signals from the last 5 shots of the lasing shots burst for each of the 10 interrogated positions of the surface of each target (individual points) is presented. As inferred, beyond the variability within ratio values, the average ratio for the set of sampling positions at each target lies close to

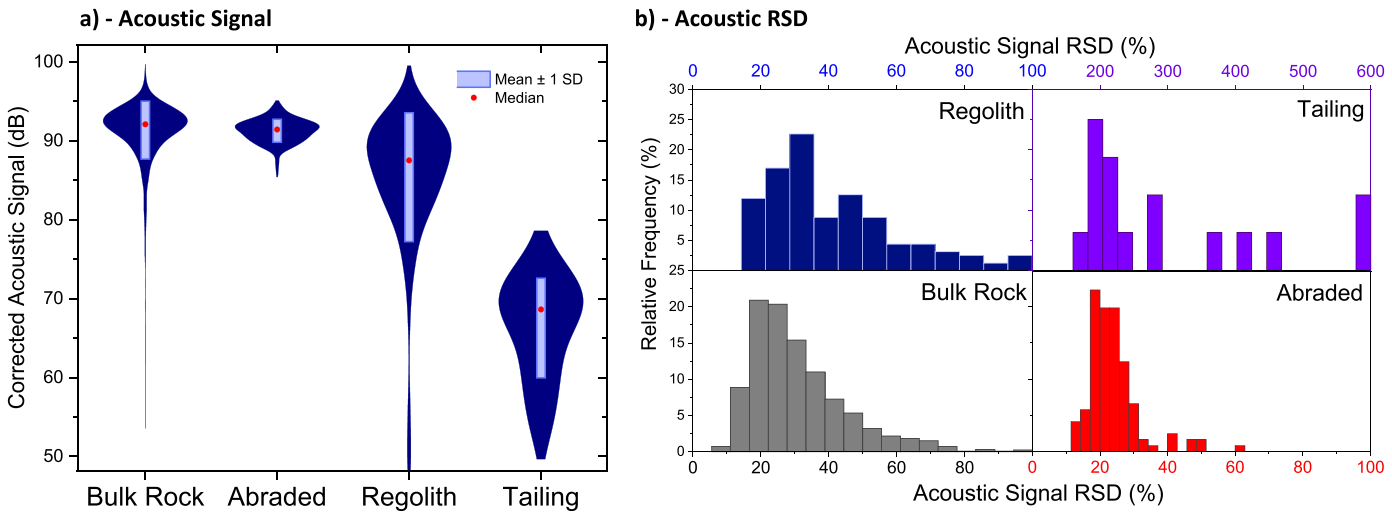

Fig. 6. A) Acoustic signal violin and box plots (red point is the median). B) Histogram for the intra-position RSD (%). (For interpretation of the references to colour in this figure legend, the reader is referred to the web version of this article.)

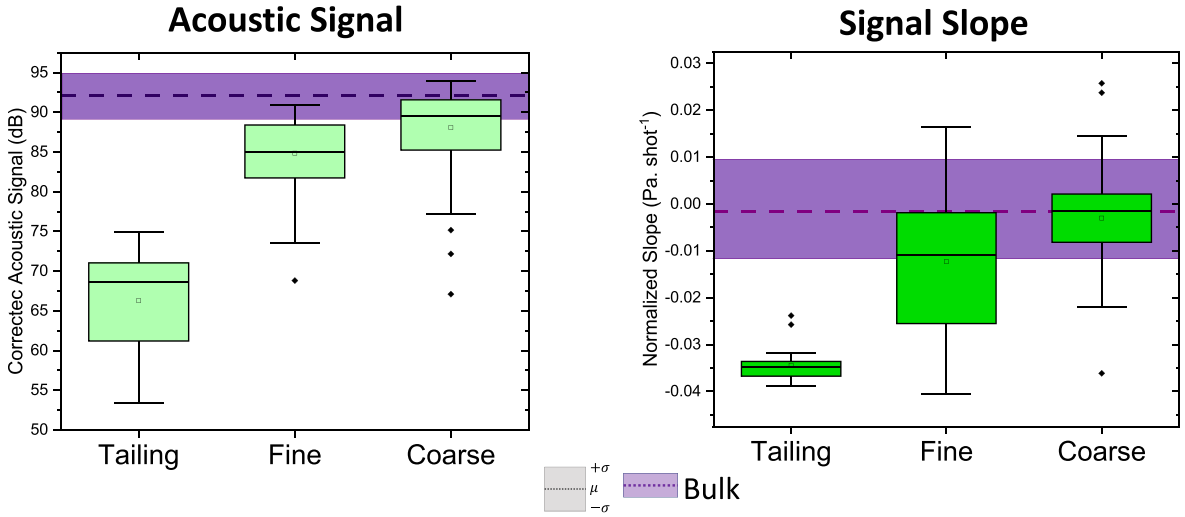

Fig. 7. Comparison of the acoustic signals for populations of "tailings" and "regolith" (split into its different traits, "fine" and "coarse"). Purple areas correspond to the mean values ±1 standard deviation for the bulk rocks class from Fig. 6. (For interpretation of the references to colour in this figure legend, the reader is referred to the web version of this article.)

unity, thereby suggesting that the acoustic signal is influenced by the underlying material. As stated, on its traverse during the first 380 Sols of the mission, the rover has investigated different geological units in the Jezero crater [19].

Thus, the next step lies on studying the acoustic signal related to these units, focusing on the "rock" and "abraded" populations, given their lower variability. Previous publications [24,25] on the composition of those geological units from LIBS and VISIR measurements together with high-resolution images from SuperCam have reported chemical compositions attributed to pure mineral phases (mainly pyroxene and olivine) for several sampling positions. Since inspected targets presenting a unique mineral phase were not common along the traverse, only targets from Séítah geological formation, involving a valuable diversity of pyroxene and olivine mineral phases, were considered. Targets from other geological units have been ignored here due to their relatively low number of observations. Fig. 8 compares the acoustic signals produced by the different targets grouped according to their inferred pyroxene and olivine compositions. The mineral stoichiometry is derived from LIBS measurements. On the one hand, pyroxene composition slight differs from Máaz (augite and Fe-rich pyroxenes) to Séítah (contains pyroxenes more enriched in Mg). On the other hand, Olivine tends to have slightly higher densities than pyroxenes for the same Fe/Mg ratio since olivine contains less Si. Because of that, olivines have higher (Fe + Mg) than pyroxenes. In general, it seems that the higher the heavy transition metal (like Fe, Ti and some other) abundances, the stronger the LIBS spark is optically and acoustically. Moreover, when the acoustic signals for pyroxenes in Séítah are compared to those produced by olivines, we found smaller data dispersion and generally higher values for olivines. While Séítah is dominated by olivine, confirmed by all three SuperCam spectral techniques, pyroxenes were identified in both the Séítah and Máaz formations [19].

Thus, in order to gain further insight into sample-related acoustic signal variations, the acoustic signal for pyroxenes observed in Máaz and Séítah were compared. Fig. 9A includes the pyroxene quadrilateral, showing stoichiometric pyroxene in those geological formations. Pyroxenes are represented as function of their coordinates in the compositional system $CaSiO_3$ (wollastonite - Wo), $MgSiO_3$ (enstatite - En), and $FeSiO_3$ (ferrosilite - Fe). As no pyroxenes exist with calcium contents greater than that of the diopside-hedenbergite joint (Wo = 50%); this truncated triangle is known as pyroxene quadrilateral. As seen, acoustic

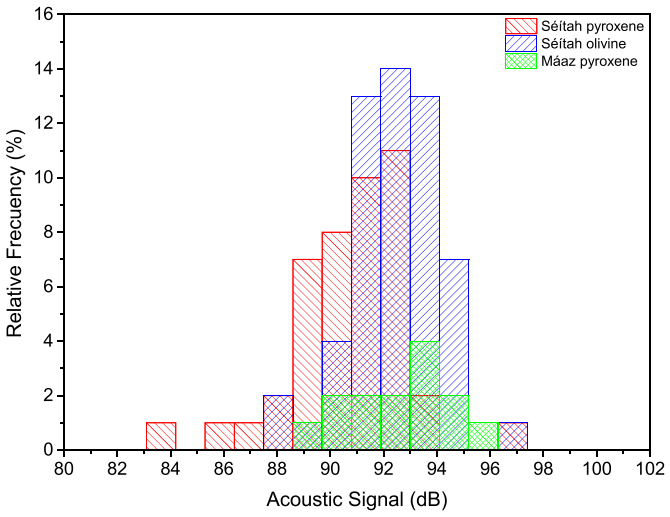

Fig. 8. Distribution of the acoustic signal for the pyroxene and olivine targets found at the Séítah and Máaz geological formations during the Perseverance path through Jezero crater floor.

intensity differences can be identified between Séítah and Máaz formations' pyroxenes. A paired comparison of the minerals in the clinopyroxene subgroup of the pyroxene group reveals that the median acoustic signal for Máaz targets is higher than the median acoustic signals for Séítah ones, Fig. 9C. The clearest example was identified from the targets labelled as clino-enstatite (for Séítah, in blue) and as clinoferrosilite (for Máaz, in green). These two pyroxene types were found only in their respective geological formations and their average acoustic signals differ significantly, at 91 ± 1 dB (0.66 ± 0.09 Pa) and 93.4 ± dB (0.94 ± 0.12 Pa) respectively. Such a difference may be linked to the distinct average density of these minerals, larger for ferrosilite (3.95 g.cm^3) as compared to enstatite (3.2 g.cm^3). In addition, in the case Pigeonite, the acoustic signal from whose targets belonging to Máaz are slightly higher in comparison with the Séítah samples, following a change in the density (3.37 ± 0.03 vs. 3.53 ± 0.04 g·cm^3). As shown in Fig. 9C, the average acoustic signal seemed to increase with the density of the mineral phase surveyed. These results agree with the ability to differentiate minerals according to their acoustic signal recently highlighted in the literature [16]. The analyses conducted during the Mars 2020 mission are exposed to workspaces governed by multiple atmospheric variables like wind, thermal fluctuations, turbulence, and dust devils, that complicate the adequate and accurate measurement of acoustic signals. In addition, the interaction of the first laser pulses with the targets can induce changes in their nature, such as the melting state

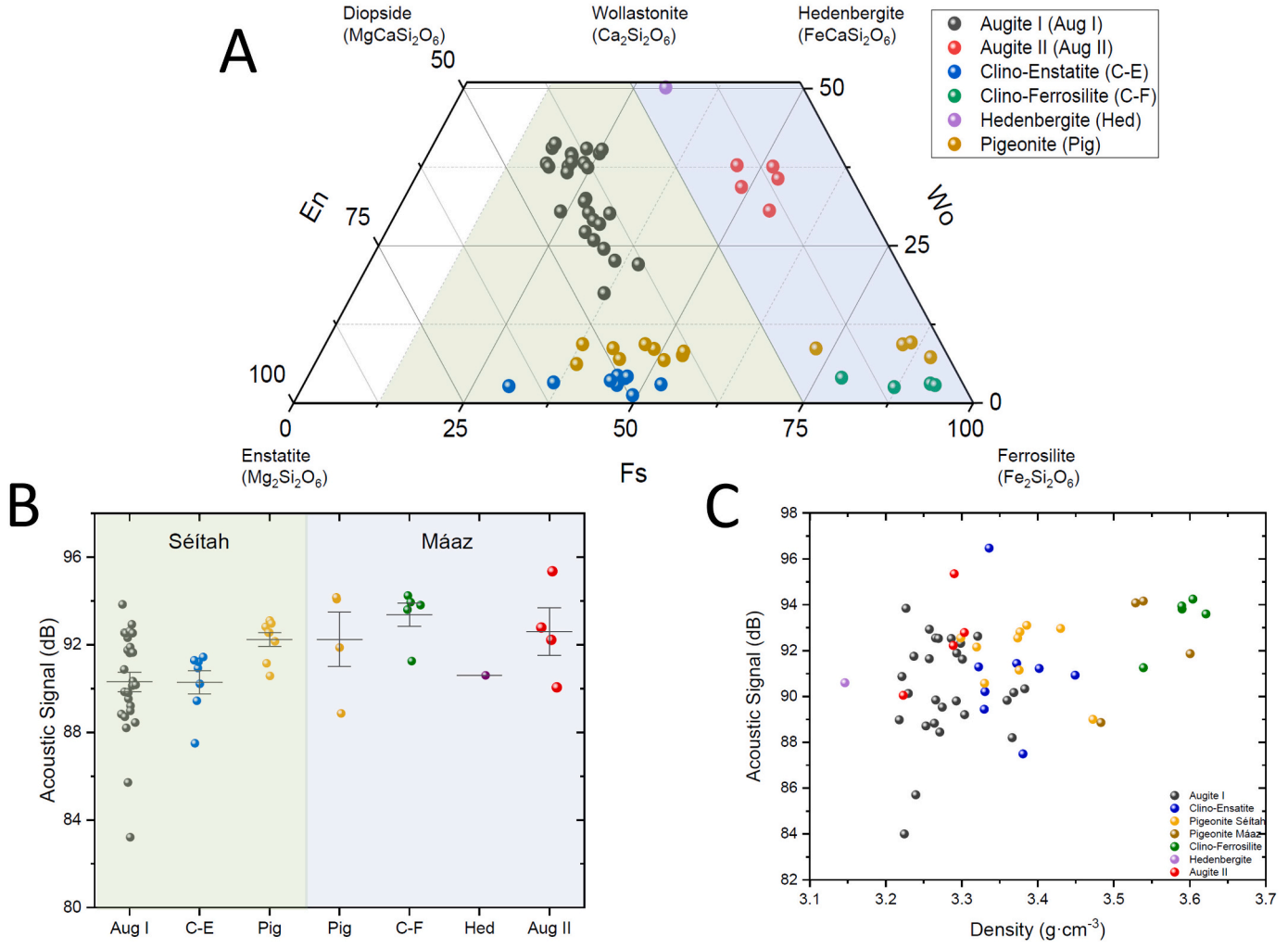

Fig. 9. A) Pyroxene quadrilateral including stoichiometric pyroxene (indicated as follows: Wo, wollastonite; En, enstatite; and Fs, ferrosilite) of the studied targets identified at those geological formations. B) Distribution and averaged acoustic signal (black line) for the pyroxenes observed in Séítah and Máaz formations. C): Evolution of the acoustic signal according the calculated target density.

of the interaction zone (depending on the target's thermal characteristics) or even changing the surface morphology and the mineral phase inside the crater [15]. All these factors, combined with the intrinsic heterogeneity of each target complicates drawing specific conclusions from any individual comparison. However, in spite of all these complexities, results herein point to the alterations/differences in the target properties translate into variations of the ensuing intensity of the laser-driven acoustic signal.

5. Conclusions

The present work evaluates, for the first time, the acoustic responses that have emerged along LIBS analysis of multiple geological targets carried out on the first 380 Sols of the Mars2020 mission at Jezero crater, Mars. The influence of the environmental conditions on the absolute intensity and reproducibility of the acoustic signals has been investigated. In particular, the target-to-rover distance and the atmospheric conditions at the time of analysis have shown to affect much more the stability of the acoustic signal as compared to that of optical emission LIBS signals. It has also been shown that small operational differences, such as the control of the focal point of laser on a target surface and the presence of dust over such a surface, do not significantly disturb the acoustic signal.

In contrast, the nature of the target surface is highlighted as a key factor when comparing the acoustic signals of different targets. The harder the surface and more compact the geological material, the louder and more stable the acoustic signal. Thus, results herein anticipate the use of this cutting-edge spectroscopy on space exploration by adding a new layer of information on the physics of geological targets to complement the chemical features provided by LIBS. Furthermore, acoustic signatures have shown synergy with the chemical differentiation between mineral phases, though still at an embryonic stage. While acoustic values are not specific for each mineral phase, acoustic variations detected between olivine and pyroxenes as well as between pyroxene populations identified at different geological formations on Mars, encourage further studies focusing on identifying different mineral phases using their relative laser-driven acoustic responses. However, several factors concerning the analysis workspace, such as the geological context and the atmospheric conditions, need to be carefully addressed to establish the links between the collected signal and the source. A study on the effect of wind, turbulence and temperature gradients on both LIBS and acoustic signals of Martian rocks is in progress.

Credit author statement

Writing—original draft: C.A-LL; P·P; J.L; J.M.

Writing—review and editing: C.A-LL; P·P; J.L; J.M, S.M, R.C.W., A. U., O.G, J.L.

Investigation/operations: All the authors.

Various members of the SuperCam Team also contributed in operations and calibrations.

Declaration of Competing Interest

The authors declare that they have no known competing financial interests or personal relationships that could have appeared to influence the work reported in this paper.

Data availability

Data will be made available on request.

Acknowledgment

Many people helped with this project in addition to the co-authors, including hardware and operation teams, and we are most grateful for their support. This project was supported in the USA by NASA's Mars Exploration Program and in France is conducted under the authority of CNES. Research funded by projects UMA18-FEDERJA-272 from Junta de Andalucía and PID2020-119185GB-I00 from Ministerio de Ciencia e Innovacion, of Spain. P.P. is grateful to the European Union's Next Generation EU (NGEU) plan and the Spanish Ministerio de Universidades for his Margarita Salas fellowship under the program ″Ayudas para la Recualificacion del Sistema Universitario Español″. RCW was funded by JPL contract 1681089. A.U was funded by NASA Mars 2020 Participating Scientist program 80NSSC21K0330.

Appendix A. Supplementary data

Supplementary data to this article can be found online at https://doi.org/10.1016/j.sab.2023.106687.

References

[1] N. Mangold, et al., Perseverance rover reveals an ancient delta-lake system and flood deposits at Jezero crater, Mars, Science 374 (2021) 711–717, https://doi.org/10.1126/science.abl4051.
[2] NASA/JPL-Caltech, Explore with Perseverance. https://mars.nasa.gov/mars2020/surface-experience/?drive=1878&site=4, 2022.
[3] Perseverance''s Location. https://mars.nasa.gov/mars2020/mission/where-is-the-rover/, 2022.
[4] K.A. Farley, et al., Mars 2020 Mission overview, Space Sci. Rev. 216 (2020) 142, https://doi.org/10.1007/s11214-020-00762-y.
[5] R.C. Wiens, et al., The SuperCam instrument suite on the NASA Mars 2020 rover: body unit and combined system tests, Space Sci. Rev. 217 (2021) 4, https://doi.org/10.1007/s11214-020-00777-5.
[6] S. Maurice, et al., The SuperCam instrument suite on the Mars 2020 rover: science objectives and mast-unit description, Space Sci. Rev. 217 (2021) 47, https://doi.org/10.1007/s11214-021-00807-w.
[7] S. Maurice, et al., The ChemCam instrument suite on the Mars science laboratory (MSL) rover: science objectives and mast unit description, Space Sci. Rev. 170 (2012) 95–166, https://doi.org/10.1007/s11214-012-9912-2.
[8] R.C. Wiens, et al., The ChemCam instrument suite on the Mars science laboratory (MSL) rover: body unit and combined system tests, Space Sci. Rev. 170 (2012) 167–227, https://doi.org/10.1007/s11214-012-9902-4.
[9] W. Xu, et al., The MarSCoDe instrument suite on the Mars rover of China's Tianwen-1 Mission, Space Sci. Rev. 217 (2021) 64, https://doi.org/10.1007/s11214-021-00836-5.
[10] S. Maurice, et al., In situ recording of Mars soundscape, Nature. 605 (2022) 653–658, https://doi.org/10.1038/s41586-022-04679-0.
[11] B. Chide, et al., Acoustics reveals short-term air temperature fluctuations near Mars' surface, Geophys. Res. Lett. 49 (2022), https://doi.org/10.1029/2022GL100333.
[12] N. Murdoch, et al., The sound of a Martian dust devil, Nat. Commun. 13 (2022) 7505, https://doi.org/10.1038/s41467-022-35100-z.
[13] N. Murdoch, et al., Laser-induced breakdown spectroscopy acoustic testing of the Mars 2020 microphone, Planet. Space Sci. 165 (2019) 260–271, https://doi.org/10.1016/j.pss.2018.09.009.
[14] B. Chide, S. Maurice, N. Murdoch, J. Lasue, B. Bousquet, X. Jacob, A. Cousin, O. Forni, O. Gasnault, P.Y. Meslin, J.-F. Fronton, M. Bassas-Portus, A. Cadu, A. Sournac, D. Mimoun, R.C. Wiens, Listening to laser sparks: a link between laser-induced breakdown spectroscopy, acoustic measurements and crater morphology, Spectrochim. Acta B At. Spectrosc. 153 (2019) 50–60, https://doi.org/10.1016/j.sab.2019.01.008.
[15] B. Chide, O. Beyssac, M. Gauthier, K. Benzerara, I. Estève, J.-C. Boulliard, S. Maurice, R.C. Wiens, Acoustic monitoring of laser-induced phase transitions in minerals: implication for Mars exploration with SuperCam, Sci. Rep. 11 (2021) 24019, https://doi.org/10.1038/s41598-021-03315-7.
[16] C. Alvarez-Llamas, P. Purohit, J. Moros, J. Laserna, LIBS-acoustic mid-level fusion scheme for mineral differentiation under terrestrial and Martian atmospheric conditions, Anal. Chem. 94 (2022) 1840–1849, https://doi.org/10.1021/acs.analchem.1c04792.
[17] K.M. Stack, et al., Photogeologic map of the perseverance rover field site in Jezero crater constructed by the Mars 2020 science team, Space Sci. Rev. 216 (2020) 127, https://doi.org/10.1007/s11214-020-00739-x.
[18] S. Holm-Alwmark, K.M. Kinch, M.D. Hansen, S. Shahrzad, K. Svennevig, W. J. Abbey, R.B. Anderson, F. Calef, S. Gupta, E. Hauber, B. Horgan, L.C. Kah, J. Knade, N.B. Miklusicak, K.M. Stack, V.Z. Sun, J.D. Tarnas, C. Quantin-Nataf, Stratigraphic relationships in Jezero crater, Mars: constraints on the timing of fluvial-lacustrine activity from orbital observations, J. Geophys. Res. Planets 126 (2021) 1–31, https://doi.org/10.1029/2021JE006840.
[19] R.C. Wiens, et al., Compositionally and density stratified igneous terrain in Jezero crater, Mars, Sci. Adv. 8 (2022), https://doi.org/10.1126/sciadv.abo3399.
[20] L. Mandon, et al., Reflectance of Jezero crater floor: 2. Mineralogical interpretation, J. Geophys. Res. Planets (2022), https://doi.org/10.1029/2022JE007450. In Press.

[21] C. Alvarez-Llamas, P. Purohit, J. Moros, J. Laserna, Differentiation of closely related mineral phases in Mars atmosphere using frequency domain laser-induced plasma acoustics, Anal. Chim. Acta 1226 (2022), 340261, https://doi.org/10.1016/j.aca.2022.340261.

[22] M. Bosáková, P. Purohit, C. Alvarez-Llamas, J. Moros, K. Novotný, J. Laserna, A systematic evaluation on the impact of sample-related and environmental factors in the analytical performance of acoustic emission from laser-induced plasmas, Anal. Chim. Acta 1225 (2022), 340224, https://doi.org/10.1016/j.aca.2022.340224.

[23] A. Petculescu, R.M. Lueptow, Atmospheric acoustics of Titan, Mars, Venus, and Earth, Icarus. 186 (2007) 413–419, https://doi.org/10.1016/j.icarus.2006.09.014.

[24] A. Udry, et al., A Mars 2020 perseverance SuperCam perspective on the igneous nature of the Máaz formation at Jezero crater and link with Séítah, Mars, J. Geophys. Res. Planets 127 (2022), https://doi.org/10.1029/2022JE007440 e2022JE007440.

[25] O. Beyssac, et al., Petrological traverse of the olivine cumulate Séítah formation at Jezero crater, Mars: a perspective from SuperCam onboard Perseverance, J. Geophys. Res. Planets (2023). Submitted.